



Middle-to-late Holocene palaeoenvironmental reconstruction from the A294 ice-cave record (Central Pyrenees, northern Spain)

Carlos Sancho^{a,*}, Ánchel Belmonte^a, Miguel Bartolomé^{a,b}, Ana Moreno^b, María Leunda^b, Jerónimo López-Martínez^c

^a Universidad de Zaragoza, Pedro Cerbuna 12, 50009 Zaragoza, Spain

^b Instituto Pirenaico de Ecología-CSIC, Avda. de Montañana 1005, 50059 Zaragoza, Spain

^c Universidad Autónoma de Madrid, Facultad de Ciencias, 28049 Madrid, Spain

ARTICLE INFO

Article history:

Received 16 July 2017

Received in revised form 3 December 2017

Accepted 10 December 2017

Available online 20 December 2017

Editor: M. Frank

Keywords:

firn ice cave

radiocarbon dating

isotopic composition

Holocene climate

Central Pyrenees

ABSTRACT

Perennial ice deposits in caves represent unique, but underexplored, terrestrial sequences that potentially contain outstanding palaeoclimatic records. Here, we present a pioneer palaeoenvironmental study of an ice deposit preserved in a small sag-type cave (A294) in the Central Pyrenees (northern Iberian Peninsula). The 9.25-m-thick sequence, which is dated from 6100 ± 107 to 1888 ± 64 cal BP, represents the oldest known firn ice record worldwide. The stratigraphy (detrital layers, unconformities, and cross stratification), plant macrofossils, and isotopic signature (similarity between the ice linear distribution, $\delta^2\text{H} = 7.83\delta^{18}\text{O} + 8.4$, and the Global Meteoric Water Line) of the ice point to the diagenesis of snow introduced to the cave by winter snowstorms. Four phases of rapid ice accumulation (6100–5515, 4945–4250, 3810–3155, and 2450–1890 cal BP) are related to wetter and colder winters. Comparison of the isotopic composition ($\delta^{18}\text{O}$ and deuterium excess) of the ice with other paleoclimate records show that both source effects and the North Atlantic Oscillation (NAO) mechanism exert a dominant influence on the ice cave record. The NAO signal may be a combination of source effects and rainfall amount. Three intervals with low ice accumulation occurred between the phases of rapid accumulation and were related to drier, and possibly warmer, winters. These centennial-scale episodes appear to be in-phase with regional arid events, as established from high altitude lacustrine records and can be correlated to global Rapid Climate Change events. The current warming trend has dramatically decreased the volume of the ice deposit in cave A294.

© 2017 Elsevier B.V. All rights reserved.

1. Introduction

Ice caves are rock cavities that host perennial ice resulting from the diagenesis of snow and/or freezing of infiltrated water (Perşoiu and Onac, 2012). Ice cave deposits are unique cryospheric archives with high palaeoenvironmental potential, based on geochemical and biological variables associated with changes in climate, vegetation, and hydrology of mid-high altitude and latitude areas (Luetscher et al., 2005; Stoffel et al., 2009; Feurdean et al., 2011; Kern and Perşoiu, 2013; Perşoiu et al., 2017). However, cave ice archives have been poorly exploited as palaeoclimatic records because of a lack of robust chronologies, difficulties in interpreting isotopic signals and detection of ablation periods in ice sequences (Luetscher et al., 2007;

Stoffel et al., 2009; Hercman et al., 2010; Feurdean et al., 2011; Spötl et al., 2014; Perşoiu et al., 2017).

In this study, we address the palaeoenvironmental significance of ice cave A294, located on the Cotiella Massif in the Southern Pyrenees. The Pyrenees form the highest calcareous mountain belt in Western Europe and ice cave A294 is the southernmost studied in Europe. The occurrence of ice caves in northern Spain has been well known since pioneering reconnaissance work in the Monte Perdido Massif (Central Pyrenees) in the mid-twentieth century. Subsequent studies of ice caves mainly focused on characterising current environmental conditions in the Pyrenees (ice cave A294) (Belmonte-Ribas et al., 2014) and Cantabrian Mountains (Peña Castil ice cave) (Gómez-Lende et al., 2014), but there has been no systematic palaeoclimatic analysis of cave ice deposits from the northern Iberian Peninsula.

Here, we present a palaeoclimatic reconstruction based on a firn ice profile in ice cave A294 which encompasses the mid- to late Holocene and is framed by a reliable radiocarbon age model. In addition, the stratigraphic architecture of the ice sequence and

* Corresponding author. Departamento de Ciencias de la Tierra, Universidad de Zaragoza, Pedro Cerbuna, 12, 50009 Zaragoza, Spain.

E-mail address: csancho@unizar.es (C. Sancho).

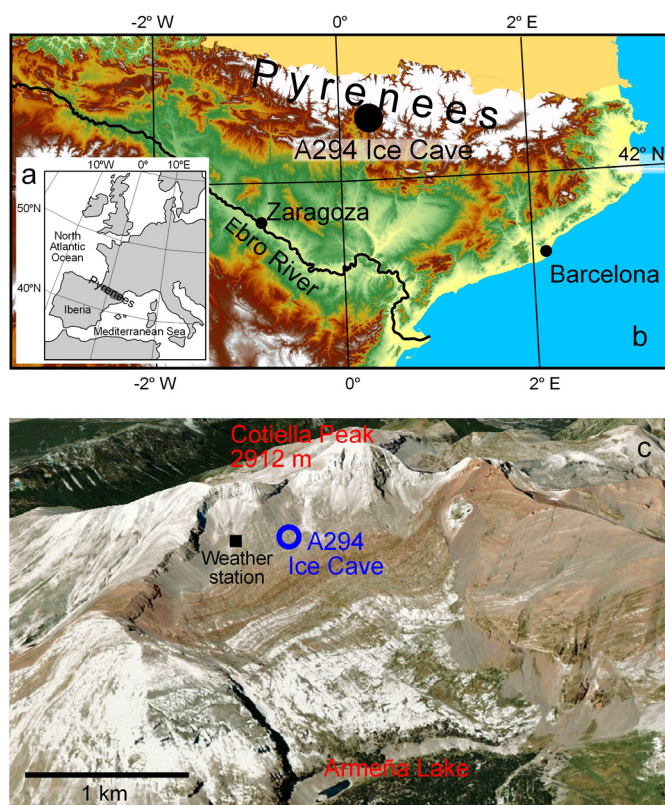


Fig. 1. Location of the A294 ice cave in northeastern Iberia (a), the Central Pyrenees (b) and the Cotiella Massif (Huesca province) (image Landsat from Google Earth 2015) (c).

its stable isotopic composition are discussed in terms of Holocene palaeoenvironmental variations.

2. Setting of cave A294

Ice cave A294 ($42^{\circ}30'52''\text{N}$; $0^{\circ}20'10''\text{E}$, 2238 m asl) is located in Cotiella, a deglaciated calcareous massif of the south-central Pyrenees (Huesca province, Northern Spain) (Fig. 1). This alpine mountain is mainly composed of Upper Cretaceous and Eocene carbonate rocks arranged in a thrust system. The cave is part of a large karst system encompassing more than 8 km of cave passages and up to 600 m deep.

Ice cave A294 opens at the bottom of a large glacial cirque and is positioned between a set of Last Glacial Maximum moraines (about 1920 m elevation) and a huge moraine complex of Younger Dryas age (2400 m). Above the moraines (2500 m), there is an active rock glacier that originated during the Little Ice Age (LIA). Periglacial activity is limited to ice-thaw processes, with remarkably little evidence of solifluction and associated morphologies (Belmonte-Ribas, 2014).

The study area experiences a mountain climate, and is situated in an air mass transition zone, with precipitation derived from both North Atlantic (Jódar et al., 2016) and Mediterranean (Araguás-Araguás and Diaz Teijeiro, 2005) systems. Meteorological observations from summer 2011 to summer 2016 were obtained from a weather station located 400 m from the cave at an altitude of 2180 m. A mean annual temperature of 1.5°C was recorded over the period, with strong seasonal contrasts (mean winter and summer temperatures of -5°C and 9.5°C , respectively). Annual precipitation of ca. 1700 mm mostly occurred as snow events, with >60 per year, concentrated between October and May, and a snow mantle thickness of up to 250 cm in March–April. Snow precipi-

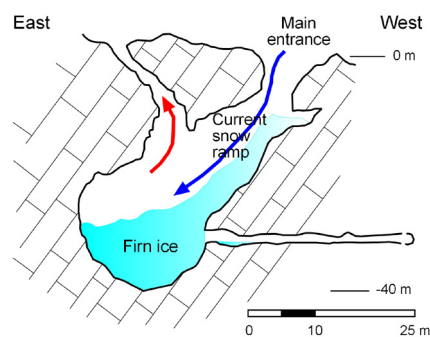


Fig. 2. Vertical cross-section of the A294 ice cave showing the ice deposit. The current air circulation pattern during winter (descending and ascending arrows are cold and warm air flows, respectively) is also shown.

tation in winter months is usually associated with the arrival of Atlantic fronts.

There is a strong altitudinal vegetation gradient in the study area, from valley bottom (1300 m) to Cotiella Peak (2912 m). Well-developed deciduous forests occur up to 1700 m, with species such as *Betula pendula*, *Corylus avellana*, and *Fagus sylvatica* that mix with conifers, such as *Pinus sylvestris*. Between 1700–2000 m, the forest is mainly composed of *Pinus uncinata* and shrubs, such as *Juniperus communis*, *Rhododendron ferrugineum*, and *Arctostaphylos uva-ursi*. Ice cave A294 is located above the present day treeline (established by *P. uncinata*) of ca. 2000 m, in a zone of patchy alpine vegetation.

A294 is a small sag-type cave (Fig. 2) with a circular entrance of approximately 30 m^2 and another smaller entrance. The chamber is triangular in plan, approximately 40 m wide and 22 m high, and hosts an ice deposit with a volume of nearly 250 m^3 . Currently, a snow ramp connects the main entrance with the top of the ice deposit, indicating that snow is blown directly into the cave (Fig. 3a). An ice wall front (ca. 10 m high) provides excellent exposures of ice stratigraphy (Fig. 4a).

The temperature and relative humidity of ice cave A294 were recorded over one annual cycle from May 2011 to May 2012 (Belmonte-Ribas et al., 2014) and show four environmental phases in terms of the relationships between climatic conditions inside and outside the cave. First, open conditions, preceded by a chimney effect (Fig. 2), occur in the cave during the winter phase (November–May), with a mean temperature of -0.77°C inside the cave. Ventilation takes place through the main shaft and out of the second smaller shaft (Fig. 2). This connection is reversed during the summer phase (June–October), and the cave acts as a thermal trap, reaching a mean temperature of 0.26°C . Transitional cooling and warming phases have also been recognized. Therefore, A294 can be considered a statodynamic ice cave following the classification of Luetscher and Jeannin (2004). The cave is currently experiencing an annual ice loss of approximately 12 m^3 , based on estimates during the years 2008–2012 (Belmonte-Ribas et al., 2014), and the ice deposit is in danger of being lost in ca. 20 years.

3. Materials and methods

Detailed logging of the well-exposed front wall of the ice deposit in cave A294 allowed us to characterize the stratigraphy. Internal stratigraphic features and unconformities were identified and described. The stratigraphic column was subsequently sampled for radiocarbon dating, using plant macro remains, and isotopic analysis.

AMS ^{14}C dating was undertaken on 22 plant macro samples, of which 5 were replicates taken from 2 horizons to assess reproducibility. Analyses were carried out at the Radiocarbon Laboratory of the University of Zürich, Switzerland, and the Radiocarbon Dating Service, Seattle, Washington, USA. Radiocarbon dates were

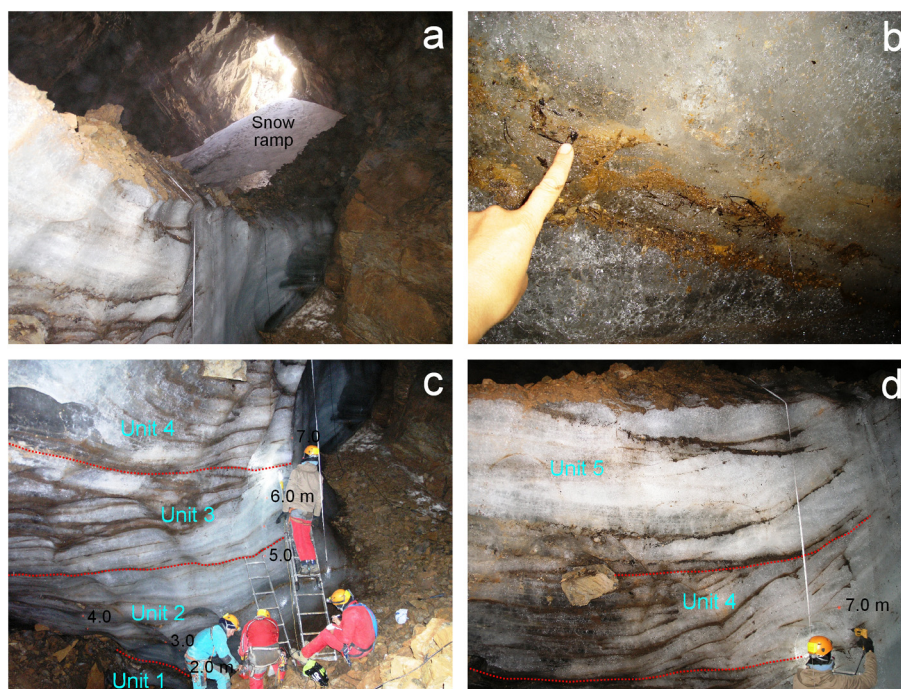


Fig. 3. Pictures from deposits inside ice cave A294. The current snow ramp overlaps the upper section of the ice deposit. An accumulation of rock fragments covers the cross-stratified ice (a). Details of minor detrital layers, including plant macroremnants (b). Ice stratigraphic units 1, 2, 3 and 4, which are differentiated in the lowermost section of the sequence (c), and units 4 and 5, which are differentiated in the uppermost section of the sequence (d). Detrital layers, unconformities and internal cross stratification can be recognized in both pictures (c and d).

Table 1
Radiocarbon data of terrestrial plant macrofossils from the A294 ice cave.

Lab ID	Sample	Detrital layer	Thickness (cm)	^{14}C age	Cal age (yr BP) 95% range
UZ-5986/ETH-44432	A294/11/-1	1	0	5320 ± 35	5993–6206
UZ-5987/ETH-44433	A294/11/0	2	40	5090 ± 40	5743–5917
UZ-5908/ETH-41311	A294-10-1	3	155	4745 ± 45	5446–5587
UZ-5909/ETH-41312	A294-10-2	4	175	4405 ± 45	4858–5069
UZ-5695/ETH-37746	A-294-2B-08	4	175	4430 ± 55	4867–5088
UZ-5910/ETH-41312	A294-10-3	5	305	4185 ± 45	4579–4771
UZ-5911/ETH-41314	A294-10-4	6	380	4060 ± 45	4423–4648
UZ-5912/ETH-41315	A294-10-5B	7	445	3885 ± 45	4222–4422
UZ-5913/ETH-41316	A294-10-6	8	495	3845 ± 45	4147–4413
UZ-5914/ETH-41317	A294-10-7	Between 8–9	505	3820 ± 45	4137–4359
UZ-5915/ETH-41467	A294-10-8B	9	515	3540 ± 35	3703–3912
UZ-5988/ETH-44434	A294-10-10	10	647	2985 ± 35	3057–3253
UZ-6042/ETH-45649	A294-10-11	11	652	2985 ± 30	3064–3246
D-AMS 013233	A294-625A	11	652	2987 ± 23	3076–3228
D-AMS 013234	A294-625B	11	652	2946 ± 28	3000–3180
D-AMS 013235	A294-625C	11	652	2945 ± 24	3004–3171
D-AMS 013236	A294-625D	11	652	2922 ± 24	2985–3159
UZ-5989/ETH-44435	A294-10-12	12	762	2990 ± 35	3060–3255
UZ-5990/ETH-44436	A294/11/13	13	772	2440 ± 35	2357–2542
UZ-5991/ETH-44437	A294/11/14	14	822	2215 ± 35	2147–2328
UZ-5992/ETH-44438	A294/11/15	15	872	2025 ± 30	1895–2060
UZ-5993/ETH-44439	A294/11/16	16	892	1950 ± 35	1824–1952

calibrated using the IntCal13 curve (Reimer et al., 2013) (Table 1). An age–depth model was built by linear interpolation between the dated levels using CLAM2.2 software (Blaauw et al., 2010). In addition, this simple model was compared to results obtained through CLAM2.2 smooth-spline interpolation and BACON Bayesian (Blaauw and Christen, 2011) age modelling approaches.

For isotopic analysis ($\delta^{18}\text{O}$ and $\delta^2\text{H}$), 180 ice microcores of 1.5 cm diameter and 5 cm length were recovered at 5-cm intervals using a homemade stainless steel crown adaptor on a drill. The resulting melted water samples were filtered in situ and sent to the Stable Isotopes Laboratory of the Mass Spectrometry Unit in the Universidad Autónoma de Madrid, Spain, for analysis. A Gas-

Bench Thermo coupled in continuous flow to a Thermo Delta V Advantage IRMS (Isotope Ratio Mass Spectrometer) was used for $\delta^{18}\text{O}$ analysis, and $\delta^2\text{H}$ was analysed by pyrolysis in an EA Thermo 1112 HT (Elemental Analyser) coupled in continuous flow to a Thermo Delta V Advantage IRMS. The results were expressed as ‰ relative to Vienna Standard Mean Ocean Water (V-SMOW), and duplicates, which were run occasionally to check for homogeneity, replicated within 0.6‰ for $\delta^2\text{H}$ and 0.07‰ for $\delta^{18}\text{O}$. Subsequently, the deuterium-excess (d-excess) was calculated following Dansgaard (1964). A number of additional samples (15 samples) were taken for isotopic analysis, from snow accumulated in the

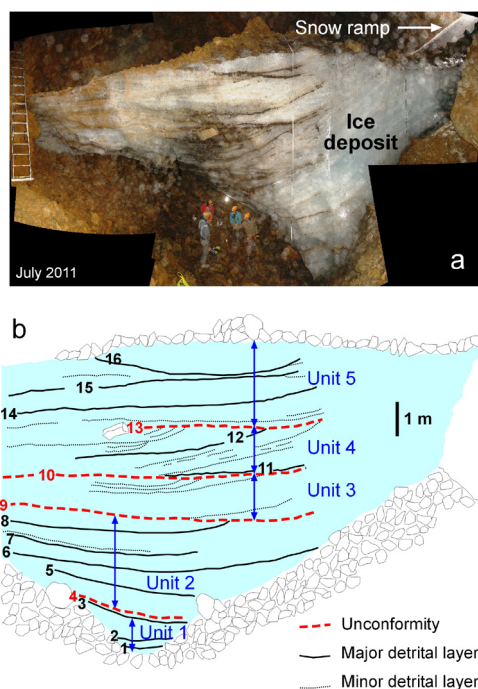


Fig. 4. Composition of photographs of the A294 ice-cave deposits taken during July 2011 (a) (the current feeding snow ramp is also indicated). The derived scheme of the ice sequence shows the general internal stratigraphic architecture of ice and unconformities and stratigraphic units, and major and minor detrital layers. Note that the thickness of units is derived from the photographs and are not adjusted to the real thickness shown in Fig. 5. Vertical scale bar is indicative. The position of the arrowed lines indicates the track that is followed to describe the stratigraphic log and sampling (b).

cave entrance, dripping water in the cave, and local precipitation (rain and snow).

4. The ice record of cave A294

4.1. Ice chronostratigraphy

The cave ice sequence comprised 9.25 m of firn ice, in which neither congelation ice deposits, lateral ice flow features nor snow avalanche structures were recognized. The stratigraphy is characterized by cross-stratified ice beds resulting from accumulation of snow entering the cave and its subsequent transformation (Fig. 4b). The ice profile includes 16 major detrital and organic-rich layers comprising cryoclastic rock fragments, fine detrital sediments, and large amounts of plant macrofossils (Fig. 3b). Exceptionally good preservation allowed identification of both arboreal and herbaceous remains that included taxa such as *Pinus uncinata*, *Abies alba*, *Vaccinium myrtillus*, *Arctostaphylos uva-ursi*, *Dryas octopetala*, and *Iris latifolia*, as well as different species of Poaceae, Caryophyllaceae, and Asteraceae, among others. Most plant macrofossils correspond with vegetation that is currently found near cave A294 and are likely to have been transported a short distance into the cave and then incorporated into the ice sequence.

The cave ice stratigraphic sequence was divided into five units based on the occurrence of unconformities (Fig. 3c and d). Some of these unconformities (paraconformities) are related to sedimentary contacts between parallel ice beds containing a high concentration of large cryoclasts (detrital layers 3 and 4), and others (disconformities) are related to erosional contacts truncating underlying ice beds (detrital layers 9, 10, and 13). The basic chronostratigraphic characteristics of the ice units are outlined below:

– Unit 1 (1.55 m thick) extends from the bottom of the sequence (detrital layer 1) to detrital layer 3 (Figs. 4b and 3c), and

exhibits parallel stratification. Detrital layer 3 thickens laterally and comprises centimetre–decimetre sized rock fragments. Radiocarbon dating of the three detrital layers provides 2-sigma calibrated ages (95% probability) of 6205–5995 cal BP for the base of the sequence (detrital layer 1) and 5445–5585 cal BP for the top of unit 1 (detrital layer 3) (Table 1).

– Unit 2 (3.60 m thick) extends between detrital layers 3 and 9 (Figs. 4b and 3c). The internal ice structure shows upward concave ice beds arranged in parallel. At the bottom of the unit, detrital layer 4 is parallel to the ice beds, thickens laterally and contains centimetre–decimetre sized rock fragments. The contact between units 1 and 2 is a paraconformity. Radiocarbon dating of the six major detrital layers in this unit provides 2-sigma calibrated ages (95% probability) of 5070–4860 cal BP for the base of the sequence (detrital layer 4) and 3910–3705 cal BP for the top (detrital layer 9) (Table 1). A replicate sample from detrital layer 4 gave a similar result (5090–4865 cal BP) (Table 1), indicating that the layer formed over a very short time period.

– Unit 3 (1.35 m thick) extends between detrital layers 9 and 10 (Figs. 4b and 3c). Detrital layer 10 is disconformable and truncates the underlying ice beds. The unit is composed of beds with internal cross stratification defined by minor detrital layers that often consist of organic macro remains and fine grained detrital deposits. Calibrated radiocarbon dates indicate the age of detrital layer 10 as 3255–3055 cal BP (Table 1).

– Unit 4 (1.2 m thick) extends between detrital layers 10 and 13 (Figs. 4b and 3d) and is bounded by disconformities. Internal cross stratification is well delineated by minor detrital layers, like unit 2. Plant macrofossil samples provide a calibrated ages of 2540–2355 cal BP for detrital layer 13 (Table 1) and 3255–3060 cal BP for detrital layer 11 (very similar to detrital layer 10). Additionally, five replicate samples from detrital layer 11 gave identical ages (Table 1), indicating a short period of formation of the layer.

– Unit 5 (1.55 m thick) extends between layer 13 and the top of the preserved perennial ice deposit (Figs. 4b and 3d), and disconformably overlies unit 4. The internal structure of the unit is characterized by parallel and cross stratification related to minor detrital layers. A radiocarbon date for detrital level 16 (Table 1), located approximately 33 cm below the surface of the ice sequence, indicates that the upper part of the deposit is younger than 1950–1825 cal BP.

4.2. Age–depth model of ice accumulation

The radiocarbon data (Table 1) indicate that the ice increases in age with depth, forming a normal stratigraphic succession, and covers 4200 years from 6100 ± 107 cal BP (detrital layer 1) to 1888 ± 64 cal BP (detrital layer 16), which encompasses the Middle–Late Holocene. Three different age models were constructed and compared. Replicate samples were not used to derive the age models. Bayesian techniques are usually better at representing the uncertainty of a chronology, but in this case, the BACON software produced a very smooth age–depth model and a uniform ice accumulation rate data, with the date from detrital layers 4, 8, and 12 as outliers, which was considered to be unrealistic. The CLAM smooth-spline interpolation provided a less smooth age model, showing changes in the ice accumulation rate over time. However, the interpolation introduced a reversal in the accumulation rate in stratigraphic unit 4. Finally, the CLAM linear interpolation was selected as the best approach since it produced a realistic chronology, with no rejection of dates or forcing of the model to give alternate periods with high and low ice deposition rates and/or ablation (Fig. 5). The periods identified in the model match well with the main stratigraphic unconformities defined in the ice deposit (Fig. 5). Hence, due to the combination of age un-

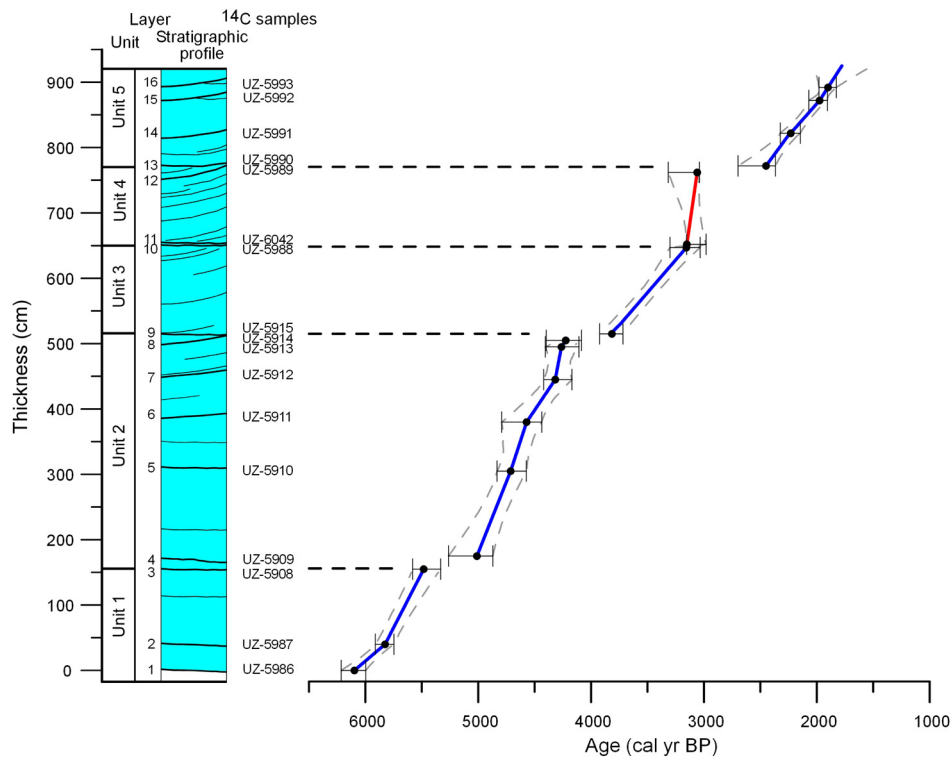


Fig. 5. Age model of the ice deposit in ice cave A294 based on linear interpolation as the best estimation according to ice stratigraphy. Note that detrital layer 12 (UZ-6042) is an exception to linear interpolation to avoid a subtle reversal (Unit 4 stretch). The stratigraphic log of the ice deposit described in the A294 cave is also shown. The thickness, main unconformities limiting stratigraphic units, major detrital layers and dated plant macroremains are indicated. Note the correspondence among unconformities and phases of the low ice accumulation rate.

certainty and match with the observed stratigraphy, we considered the CLAM linear interpolation the most reliable age–depth model.

The age–depth model was applied between detrital layers 1 and 16. Layer 1 coincides with the bottom of the stratigraphic profile but there is 33 cm of undated ice above layer 16. The age of the current surface of the ice profile was estimated as ca. 1780 cal BP through extrapolation of the age–depth model.

The age–depth model suggests variations in the ice accumulation rate over time, with several alternating multicentennial periods of high and low rates of ice deposition. Four periods of rapid ice accumulation can be identified and three stages of low accumulation. The first (6100 to 5515 cal BP) and second (4945 to 4250 cal BP) periods of rapid accumulation showed rates of 0.266 and 0.473 cm/yr, respectively. The third stage of rapid ice accumulation (3810 to 3155 cal BP) had an overall rate of 0.210 cm/yr, but rates differed between the upper and lower parts of the stage. The lower part had a lower ice accumulation rate, while the upper part, which is 1.10–1.15 m thick and includes detrital layers 10, 11, and 12, is has a uniform age making it difficult to determine the actual accumulation rate. However, ice accumulation rates must have been very high in the latter period, denoting a very rapid response of the ice depositional system. Finally, the fourth stage (2450 to 1890 cal BP) had a mean ice accumulation rate of 0.213 cm/yr.

The first phase of low ice accumulation (5515 to 4945 cal BP) is stratigraphically related to a paraconformity that is well delineated by detrital layer 4 (bottom of stratigraphic unit 2). The second stage (4250 to 3810 cal BP) correlates with the top of stratigraphic unit 2 and coincides with an erosive surface (disconformity) (detrital layer 9) truncating the underlying ice beds. Detrital layer 10 designates a disconformity that separates ice stratigraphic units 3 and 4, but does not involve a relevant gap in ice accumulation. Finally, the third stage of low ice accumulation (3155 to 2450 cal BP) correlates with the disconformity displayed by detrital layer 13, which erodes the top of stratigraphic unit 4.

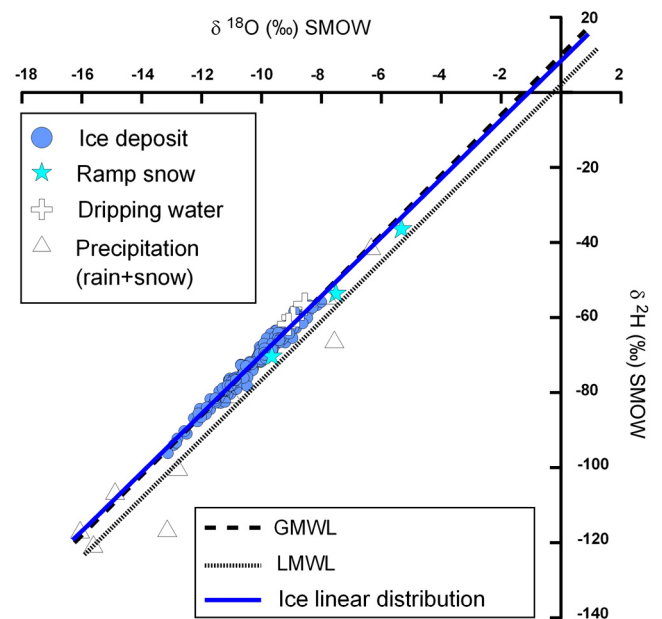


Fig. 6. Isotopic projection of the A294 ice-cave samples and resulting linear relationship, which is very close to the Global Meteoric Water Line (GMWL). The isotopic composition of precipitation in the area (November–2011 to February–2012), dripping water, and ramp snow in cave A294 (August–2011) (Belmonte-Ribas et al., 2014) are also plotted.

4.3. Ice isotopes

The stable isotope ($\delta^{18}\text{O}$ and $\delta^2\text{H}$) content of the ice samples is plotted in a scatter diagram (Fig. 6). The concentration of $\delta^{18}\text{O}$ (VSMOW) ranges from -8.01 to -13.13 ‰, with a mean of -10.21 ‰ and a standard deviation of 1.05 ‰. With respect to $\delta^2\text{H}$ (VSMOW),

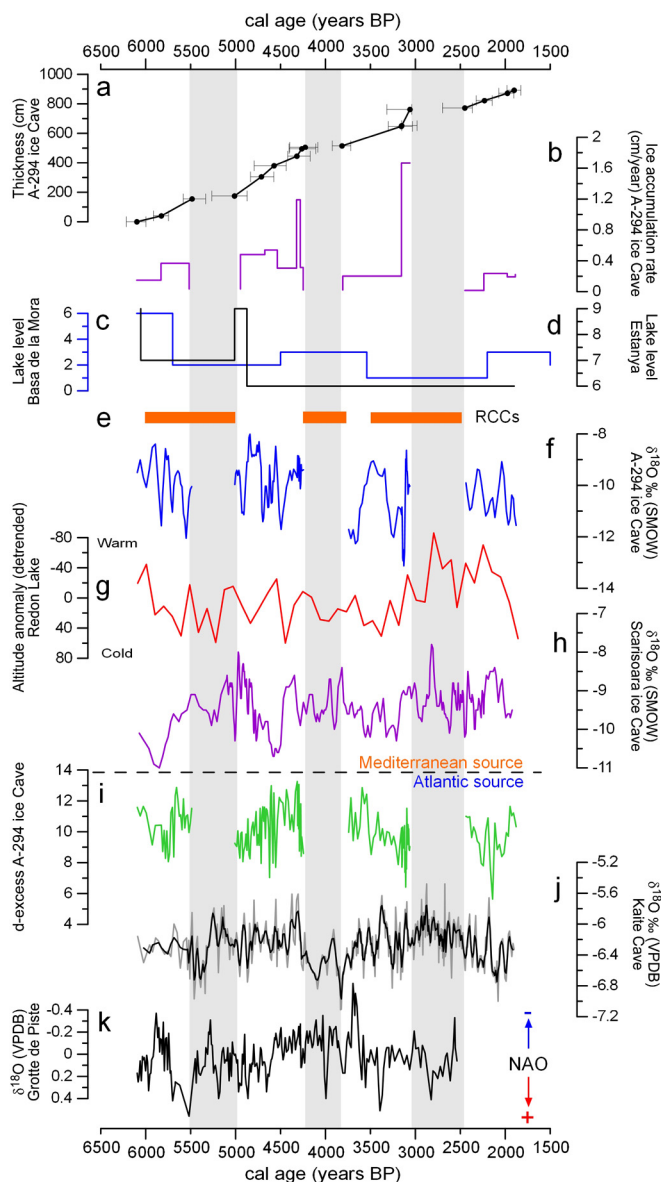


Fig. 7. Regional palaeoclimatic significance of the A294 cave-ice deposit. Age model of ice formation from linear interpolated radiocarbon dates on plant macroremains (a). Phases of the high ice accumulation rate. Intervals of the low ice accumulation rate and/or ablation are represented with vertical grey bars (b). La Basa de la Mora Lake level fluctuations, Pyrenees, Spain (González-Sampériz et al., 2017) (c). Estanya Lake level fluctuations, Pyrenees, Spain (Morellón et al., 2009) (d). Holocene rapid climate changes (Mayewski et al., 2004) (e). Variability in the $\delta^{18}\text{O}$ isotopic composition of the A-294 ice deposit (f). The cryophyte-based climate reconstruction from Pyrenean Redon Lake, Spain (Pla and Catalan, 2005) (g). Scărișoara ice cave $\delta^{18}\text{O}$ record, Romania (Perșoiu et al., 2017) (h). Variability in the d-excess from the A294 ice sequence (i). $\delta^{18}\text{O}$ speleothem record from Kaite cave, Spain (Domínguez-Villar et al., 2017) (j). Detrended $\delta^{18}\text{O}$ speleothem record from Grotte de Piste, Morocco, NW Africa, that reflects the state of the NAO (Wassenburg et al., 2016) (k).

concentrations range from -55.80 to -96.10‰ , with a mean of -71.58‰ and standard deviation of 8.38‰ . In terms of d-excess, values range from a maximum of 13.26 to a minimum of 5.64 (Fig. 7i), with a mean of 10.07 and standard deviation of 1.40 .

A linear relationship can be applied to the cave ice oxygen and hydrogen isotope data ($\delta^2\text{H} = 7.83\delta^{18}\text{O} + 8.4$) (Fig. 6), which is very similar to the Global Meteoric Water Line (GMWL, $\delta^2\text{H} = 8\delta^{18}\text{O} + 10$) (Craig, 1961). Isotopic data from local precipitation (snow and rainfall), recent snow from the ramp inside the cave, and dripping water are also plotted on the $\delta^{18}\text{O}$ – $\delta^2\text{H}$ diagram, and

follow the same linear distribution (Fig. 6) (Belmonte-Ribas et al., 2014). However, the profiles of $\delta^{18}\text{O}$ and d-excess display very high variability at the centennial scale, with no clear trend through the sequence (Fig. 7f, i).

5. Discussion

5.1. Origin of the cave ice deposit

The mode of occurrence of the ice deposit in cave A294 points to snow diagenesis as its main origin. This preliminary assumption is supported by ice stratigraphic features and isotopic composition.

5.1.1. Ice depositional architecture

One of the outstanding stratigraphic features of the A294 ice cave sequence is the presence of detrital layers composed of cryoclasts and plant macrofossils that highlight the internal cross stratification and major stratigraphic unconformities of the ice deposit (Figs. 4a, b and 3c, d). Although the presence of ice cross-stratified structures implies transport of snow, the snow depositional mechanism remains unknown. Lateral and longitudinal changes in the location of windblown snow deposition must be considered to explain the vertical aggradation of the sequence and internal architecture of the ice deposit. Varying location of snow deposition has been observed in some ice cave entrances in other Pyrenean sites currently under investigation by the present authors.

Another interesting question is the length of time needed to form a detrital layer. According to Stoffel et al. (2009) and Spötl et al. (2014), individual detrital layers represent major gaps or hiatuses in ice accumulation and major phases of ice ablation, favouring the concentration of cryoclasts as well as plant macrofossils. Although these layers may record annual summer ablation (Luetscher et al., 2007), they more commonly represent decadal-centennial periods of enhanced prevailing summer ablation processes. The elapsed time to generate a detrital layer can be constrained using the scattering of dates derived from multiple samples taken in the same layer (Stoffel et al., 2009). In ice cave A294, two samples from detrital layer 4 provided very similar calibrated ages, and five samples from detrital layer 11 offered calibrated ages ranging from 3155 ± 91 cal BP to 3072 ± 72 cal BP (Table 1). Both set of dates provide evidence that the detrital layers represent very short ablation periods (decadal time scale at a maximum). However, intensive deposition of organic remains during heavy winter storms cannot be discounted. Overall, the detrital layers represent only minor gaps considering the total time period recorded in the A294 cave ice sequence. However, detrital layers that overlie eroded ice beds delineate main stratigraphic unconformities that represent longer periods of elapsed time and separate four phases of high ice accumulation rates (Figs. 5 and 7a).

5.1.2. Isotopic composition of ice

The isotopic composition of cave ice is related to the local isotopic signal of the parent water (mainly snowfall) and, consequently, it preserves a record of regional precipitation $\delta^{18}\text{O}$. Nevertheless, the processes controlling the transfer of the isotopic signal to cave ice are neither well known nor simple (Luetscher et al., 2007; Kern et al., 2011; Yonge and MacDonald, 2014; Gradziński et al., 2016). The similarity of the linear relationship between $\delta^{18}\text{O}$ and $\delta^2\text{H}$ for the A294 cave ice deposit with the GMWL (Craig, 1961) (Fig. 6) indicates that congelation processes are not relevant in the ice origin (Gradziński et al., 2016). Furthermore, the Local Meteoric Water Line ($\delta^2\text{H} = 7.72\delta^{18}\text{O} + 0.6$), including rainfall and snowfall, as reported by Belmonte-Ribas et al. (2014) is parallel to the isotopic linear distribution of A294 ice (Fig. 6), which also indicates the absence of isotopic fraction-

ation during ice formation (Kern et al., 2011; May et al., 2011; Perşoiu et al., 2011). Consequently, we can exclude any process leading to isotopic fractionation in the formation of A294 ice other than equilibrium. The difference in the intercept of the $\delta^{18}\text{O}$ – $\delta^2\text{H}$ plots (0.6 for the Local Meteoric Water Line versus 8.4 in the ice samples) is probably related to the low number of present day rain and snowfall samples analysed, giving inadequate representation of seasonal and interannual variability.

Snow from the ramp from cave A294 shows incipient features of diagenesis and represents an intermediate stage between snowfall and firn ice (Bini and Pellegrini, 1998). Furthermore, the position of dripping water in the $\delta^{18}\text{O}$ – $\delta^2\text{H}$ diagram (Fig. 6) suggests that the transformation of snowfall-firn-ice could be governed by the wetting of snow by dripping water and subsequent freezing inside snow voids (Luetscher and Jeannin, 2004; Stoffel et al., 2009). In addition, we cannot discard a significant role for rainfall in the wetting of snow as the top of the snow ramp is directly exposed to open sky. However, on balance, the isotopic composition of the ice deposit points to snow diagenesis as the main origin of A294 cave ice; the cave acts as a natural sink, trapping windblown snow during winter storms.

5.2. Age of the cave ice deposit

Different methods and techniques may be applied to date cave ice deposits (Luetscher et al., 2007). The Scărișoara ice cave (Romania) (Perşoiu et al., 2017) has the oldest known age (radiocarbon age of 9110 ± 50 ^{14}C yr BP) and the longest span (approximately 10000 yr) for any ice cave record. Most other ice caves in Europe (e.g. Luetscher et al., 2007; Kern et al., 2009; Hercman et al., 2010; May et al., 2011; Gradziński et al., 2016) and North America (Lauriol and Clark, 1993) contain centennial-scale ice sequences younger than 2000 yr. Published ice cave chronologies are mainly derived from congelation deposits, and chronological information from firn ice deposits in caves is very limited. Stoffel et al. (2009) obtained dates ranging from 1200 ± 50 to 190 ± 45 ^{14}C yr BP for organic material in firn ice in the St. Livres ice cave (Switzerland). Similarly, Spötl et al. (2014) provided reliable ages ranging between 2664 ± 32 and 250 ± 24 from a firn-ice section from the Hundsalm ice cave (Austria).

We estimate that the A294 ice cave houses the oldest studied firn ice record worldwide (from 6100 ± 107 to 1888 ± 64 cal BP) (Table 1; Figs. 5 and 7a). The time window of the ice cave sequence seems also to be one of the longest published to date, spanning more than 4 kyr. Surprisingly, A294 cave ice does not contain any deposit corresponding to the LIA. It could be that any ice that accumulated in the Pyrenees during that cold and wet period (e.g. Morellón et al., 2012) melted afterwards. However, it is also possible that the cave entrance was blocked as result of the intense and frequent winter snowfalls associated with the LIA, preventing the ingress of snow into the cavity.

5.3. Regional palaeoclimatic significance of the cave ice deposit

Palaeoenvironmental information from the A294 ice cave sequence can be inferred from the successive phases of high and low rates of ice accumulation as well as from isotopic variability (Fig. 7b, f, and i).

5.3.1. Phases with low rates of ice accumulation in A294: a record of arid (and warm?) events in the Pyrenees

Three main phases of low ice accumulation were identified in the A294 ice cave deposit, at 5515–4945, 4250–3810, and 3155–2450 cal BP (Figs. 5 and 7a, b). The lower boundary of the phases may not represent exactly when the dry/warm period was initiated due to unknown ice ablation. In addition, the A294 ice

cave deposit does not cover the last 2000 yr, most likely due to the increased temperature of the Pyrenees in that period compared to the more stable temperature earlier in the Holocene (Mauri et al., 2015).

Phases of low ice accumulation, involving very low deposition rates and ablation processes, indicate equilibrium or negative annual mass balances (Stoffel et al., 2009) and point to arid periods and/or warmer temperatures. Conversely, high accumulation phases involve positive annual mass balances in the ice deposit (Luetscher et al., 2007), which in turn, requires substantial snowfall precipitation during wet winters (Stoffel et al., 2009). Unfortunately, there are very few palaeoclimate records available for similar altitudes and periods in the Pyrenees with which to compare the A294 cave ice record. Three lacustrine palaeoclimate sequences, from Basa de la Mora, Redon, and Estanya, are the most comparable with the A294 record and are discussed below.

Basa de la Mora Lake, located on the Cotiella massif at 1914 m altitude, is the nearest paleoclimate sequence to the A294 ice deposit. Multi proxy studies defined two phases of low lake levels, at 5.7 ka cal BP and from 2.9–2.4 ka cal BP (Pérez-Sanz et al., 2013; González-Sampériz et al., 2017) (Fig. 7c), which roughly correlate to the first and the third phases of low ice deposition in the A294 ice cave record, respectively, while the second phase is not reflected in the lake record. At a lower altitude (670 m asl), the Estanya lake record shows a high sensitivity to the arid Mid Holocene (Fig. 7d) (Morellón et al., 2009). Thus, the first period of low accumulation rates in A294 (5.5–5 ka) is very well detected in the Estanya lacustrine sequence. The two later dry phases (4250–3810 and 3155–2450 cal BP) in A294 are recorded as a prolonged period of low lake level, likely due to the lower sensitivity of the lacustrine system once it experiences a dry period (Fig. 7d). In a reconstruction of winter–spring temperature based on analysis of cryophytes from Redon Lake, located in the Central Pyrenees at an altitude of 2240 m asl (Fig. 7h), the warmest period recorded (3–2.5 kyr) coincides with the third period of low ice accumulation in cave A294. Despite the relative paucity of records, there does seem to be regional coherence to support the link between phases of low ice accumulation and winter aridity and, possibly, temperature change. Nevertheless, there is a need for more palaeoclimate records from high altitude locations in the Pyrenees that are sensitive to rapid climate changes in order to fully understand the sequence of dry events in this particularly vulnerable region.

Several phases of rapid climate change (RCCs) with global significance have been defined in the Holocene, based on comparison of different palaeoclimate records (Mayewski et al., 2004). Interestingly, the three main periods of low ice accumulation and/or ablation seen in the A294 cave record correspond well with three RCCs (6000–5000, 4200–3800, and 3500–2500 yr BP) (Fig. 7e) that are characterized by “cold poles and dry tropics” (Mayewski et al., 2004). Mechanisms to explain the effect of RCCs in the Pyrenees are not yet clear, but the three RCCs identified above have been characterized as dry events in numerous records for the Mediterranean region. Fletcher and Zielhofer (2013) showed that the West Mediterranean was relatively dry in the RCCs dating to 6000–5000 and 3500–2500, although other studies (e.g. Burg peat-bog, located at the Eastern Pyrenees at an altitude of 1821 m asl, Pelachs et al., 2011) have interpreted these as humid periods. Pollen contents from core MD95-2043 in the Alboran Sea, West Mediterranean, indicate episodes of forest decline at 5.4–4.5 and 3.7–2.9 kyr (Fletcher et al., 2013), which, allowing for chronological uncertainty, correspond with phases of low ice accumulation in the Pyrenees from our study. Although Fletcher et al. (2013) do not recognize the 4200–3800 event, this dry phase is well-recorded in many other climate records from the West Mediterranean (e.g. Ruan et al., 2016; Zielhofer et al., 2017). Although the timing of regional dry phases in the West Mediterranean sometimes slightly

differ from phases of low ice accumulation in cave A294, this difference can be explained by local climate variations, non-linear responses of proxies to climate parameters, age model uncertainties, and the potential temperature effect on ice accumulation.

5.3.2. Variability of $\delta^{18}\text{O}$ in the A294 ice sequence

5.3.2.1. Which season is being recorded in the A294 ice sequence? Several interpretations of the A294 $\delta^{18}\text{O}$ profile (Fig. 7f) arise from comparison with currently available data. Considering conservation of the precipitation signal in the ice $\delta^{18}\text{O}$ after discarding kinetic processes, observed oscillations can be associated with temperature changes, source effects or variations in the amount of precipitation (amount effect) (Rozanski et al., 1993). In high altitude areas of Europe such as the Alps, temperature change dominates over rainfall amount in shaping the precipitation $\delta^{18}\text{O}$ values (Schürch et al., 2003). Regardless of whether temperature change or precipitation amount is the dominant effect, we first need to discern which season is better represented in the ice sequence.

Presently, $\delta^{18}\text{O}$ concentrations in winter precipitation vary between -15 and -10‰ , as recorded in the only high altitude Pyrenean site (2200 m asl) where rainfall is systematically collected, namely, the Góriz mountain hut (Jódar et al., 2016), located 27 km northwest of A294 ice cave in the Ordesa and Monte Perdido National Park. At Góriz, seasonally averaged $\delta^{18}\text{O}$ and $\delta^2\text{H}$ (Jódar et al., 2016) plot very close to the GMWL with $\sim 10\text{‰}$ d-excess, indicating a dominant Atlantic origin of precipitation. Therefore, we can conclude that the ice deposit from cave A294, with $\delta^{18}\text{O}$ values of -13 and -8‰ , is mostly derived from winter precipitation when Atlantic fronts are the usual synoptic situation. Additionally, since the A294 ice sequence is derived from snow diagenesis, and it is mostly during winter that snow will enter the cavity, we expect the record to be biased towards the winter season. Discerning if temperature or precipitation dominates in the isotopic signal requires further reasoning.

5.3.2.2. Discerning the effect of temperature First, a rough calculation of the temperature change associated with the 3.5‰ of $\delta^{18}\text{O}$ variation at the centennial scale in the A294 ice sequence (Fig. 7f) is calculated. Assuming a temperature change of 0.6‰C/‰ , based on high altitude stations in Switzerland (Schürch et al., 2003), gives a temperature range of 2.1‰C for some of the major $\delta^{18}\text{O}$ oscillations. A climate reconstruction based on European pollen data (Mauri et al., 2015) indicates stable winter temperatures for southern Europe during most of the Holocene, with a warming of about 2‰C in the last two millennia. Unfortunately, the reconstruction cannot account for with the high frequency changes (decadal-centennial) that are represented in the A294 sequence, although a winter temperature variation of ca. 2.1‰C appears to be outside the range of centennial-scale changes during the Holocene. The cryophyte-based climate reconstruction from Redon Lake (Pla and Catalan, 2005) (Fig. 7g) provides a good Pyrenean temperature record, albeit biased towards the end of winter to the beginning of spring. In general, the records from A294 and Redon Lake are not in good agreement (Pearson coefficient 0.077, p value = 0.3). Additionally, comparison with the recently published Scărișoara ice cave $\delta^{18}\text{O}$ record (Romania), that is also interpreted to be dominated by winter temperature variability (Perșoiu et al., 2017) (Fig. 7h), reveals a lack of similarity with A294 record (correlation coefficient $\sigma_2 = -0.081$; $p = 0.28$). Thus, although it is true that temperature variations in Romania are not necessarily linked to those in the Pyrenees, we need to consider additional factors to explain the $\delta^{18}\text{O}$ record in ice cave A294.

5.4. Role of precipitation amount and source effects in isotopic variability

Alongside temperature, ice isotopic composition may be affected by other parameters such as precipitation amount, rain-out effects and/or changes in the moisture source. To discern the role of these mechanisms in the $\delta^{18}\text{O}$ variability of A294, other records such d-excess are discussed below.

Values of d-excess in the A294 profile range from 5.5 to 13.5‰ , with an average of 10‰ (Fig. 7i), but a high degree of noise mean it is not easily compared to the oxygen isotope record. However, the average d-excess levels of 10‰ point to an Atlantic origin of the precipitation (e.g. Araguás-Araguás and Diaz Teijeiro, 2005), making a significant Mediterranean origin for snowfall in the area unlikely. However, some peak d-excess values approach 14‰ (Fig. 7i), particularly around 4.2 ka cal BP, indicating a possible major contribution of moisture with a western Mediterranean origin (Celle-jeanton et al., 2001) during that period.

A new $\delta^{18}\text{O}$ speleothem record from Kaite Cave in the southern Cantabrian Mountains (Domínguez-Villar et al., 2017) highlights the importance of source origin in precipitation $\delta^{18}\text{O}$ values (Fig. 7j). Domínguez-Villar et al. (2017) interpret millennial-scale $\delta^{18}\text{O}$ anomalies in a composite speleothem sequence as a proxy for the zonal displacement of pressure fields over the North Atlantic; thus, a westward shift in the location of pressure fields relates to less negative $\delta^{18}\text{O}$ values. Correlation between the A294 ice record and the Kaite speleothem is low but statistically significant ($\sigma_2 = -0.19$; $p = 0.01$), thus indicating the potential of precipitation (source effect) as the main mechanism shaping $\delta^{18}\text{O}$ variability in ice cave A294. In summary, the source effect, which probably incorporates a mixture of the influence of tropical versus northern North Atlantic water masses (Domínguez-Villar et al., 2017) and those with a Mediterranean component, played a role in determining the $\delta^{18}\text{O}$ of snow precipitation in the Central Pyrenees during the Middle–Late Holocene.

The role of the second potential mechanism, precipitation amount, is now evaluated. We propose that during periods of enhanced snowfall, $\delta^{18}\text{O}$ values would be more negative, representing periods characterized by wetter winters. In Europe, the North Atlantic Oscillation (NAO) controls a significant proportion of the observed variation in the amount of winter precipitation (Trigo et al., 2002), with negative NAO winters associated with more abundant precipitation in the Pyrenees (López-Moreno et al., 2011). Changes in the state of the NAO may also be associated with moisture source variability. Comas-Bru and McDermott (2014) demonstrated that the geographical locations of NAO centres of action were modulated by other teleconnections, such as the EA (Eastern Atlantic) index. The longest, high resolution, of past NAO variations, is based on a $\delta^{18}\text{O}$ profile from a Moroccan stalagmite (Wassenburg et al., 2016) (Fig. 7k). Correlation between the A294 $\delta^{18}\text{O}$ record and the NAO reconstruction is higher than for the other records discussed and is positive (Pearson coefficient of 0.23; p value = 0.005), pointing to a connection between the NAO mechanism and wetter winters in the study area during the Middle–Late Holocene.

In summary, we have established that source effects are likely to have affected the $\delta^{18}\text{O}$ composition of the A294 ice sequence. The role of precipitation amount needs to be further examined in a monitoring and sampling programme.

6. Conclusions

Cave A294, located in the Central Pyrenees (Northern Iberia), is the southernmost ice cave in the highest karstified mountains in Europe. In this study, we have integrated analysis of the strati-

graphic features, chronology, and isotopic composition of the ice sequence and draw the following conclusions:

- The A294 ice cave preserves a firn ice sequence that is 9.25 m thick, with an internal stratigraphy that is well delineated by detrital and plant macrofossil-rich layers displaying cross-stratified ice beds and unconformities. The isotopic ice linear distribution ($\delta^2\text{H} = 7.83\delta^{18}\text{O} + 8.4$), which is very similar to the GMWL, indicates that no relevant fractionation processes occurred during ice formation. The depositional and isotopic features identified point to an origin from the diagenesis of snow introduced to the cave during winter snowstorms.
- The age of the A294 ice cave sequence ranges from 6100 \pm 107 (bottom) to 1780 cal BP (extrapolated age of the top) and, consequently, records a time period of approximately 4.3 kyr. Thus, ice cave A294 houses the oldest known firn ice record worldwide.
- Four multicentennial phases with higher ice accumulation rates are identified, at 6100–5515, 4945–4250, 3810–3155, and 2450–1890 cal BP. The phases are separated by stages of lower accumulation, including ablation processes, that mainly coincide with the main stratigraphic unconformities. Comparison with RCCs and well-known lacustrine sequences at a regional scale show that the periods of low ice accumulation are related to drier winter conditions, although the potential effect of warmer temperatures cannot be totally discarded. Our data, and comparison with other climate records, show that the climate system of the Pyrenees is complex and this may partly explain off-sets and differences between the local climate records.
- Large variation in the $\delta^{18}\text{O}$ profile at the centennial scale (3.5‰, which represents approximately 2 °C), together with a low correlation with regional palaeotemperature reconstructions, points to changes in snowfall and source area as additional factors modulating the variation of $\delta^{18}\text{O}$ in the ice sequence.
- Average ice profile d-excess values of ca. 10‰ point to the Atlantic Ocean as the dominant source of precipitation. Coherently, the NAO mechanism would have exerted a dominant influence on the amount of winter precipitation, and through changes in the moisture sources, as suggested by the good correlation between the A294 $\delta^{18}\text{O}$ record and available regional reconstructions.

This paper provides a pioneering study that demonstrates the palaeoenvironmental significance of perennial ice cave deposits in Iberia, and augments the limited palaeoclimatic dataset of high altitudes in the western Mediterranean during the Middle–Late Holocene.

Acknowledgements

This work was supported by the Spanish Government and the European Regional Development Fund (projects CGL2009-10455/BTE, CTM2013-48639-C2-1-R and CGL2016-77479-R). This is a contribution by PaleoQ and Geomorfología y Cambio Global groups (Aragón Government and European Social Fund) and IUCA (University of Zaragoza). We thank Ramón Queraltó, Carles Pons (ACEC), and Eduardo Bartolomé for their technical support and Mikel Calle, Pablo Santolaria, and Alberto Bosque for their collaboration during the fieldwork. We are also grateful to two anonymous reviewers for their helpful comments and constructive criticism that greatly improved the manuscript.

References

- Araguás-Araguás, L.J., Diaz Teijeiro, M.F., 2005. Isotope composition of precipitation and water vapour in the Iberian Peninsula. In: *Isotopic Composition of Precipitation in the Mediterranean Basin in Relation to Air Circulation Patterns and Climate*. International Atomic Energy Agency TECDOC-1453, Vienna, Austria, pp. 173–191.
- Belmonte-Ribas, A., 2014. Geomorfología del macizo de Cotiella (Pirineo oscense): cartografía, evolución paleoambiental y dinámica actual. Ph.D. thesis Universidad de Zaragoza. 581 p.
- Belmonte-Ribas, A., Sancho, C., Moreno, A., López-Martínez, J., Bartolomé, M., 2014. Present-day environmental dynamics in ice cave A294, Central Pyrenees, Spain. *Geogr. Fis. Din. Quat.* 37, 131–140.
- Bini, A., Pellegrini, A., 1998. Depositi du ghiaccio e neve. *Geol. Insubrica* 3, 89–100.
- Blaauw, M., Christen, J.A., 2011. Flexible paleoclimate age-depth models using an autoregressive gamma process. *Bayesian Anal.* 6, 457–474.
- Blaauw, M., Wohlfarth, B., Christen, J.A., Ampel, L., Veres, D., Hughes, K.A., Preusser, F., Svensson, A., 2010. Were last glacial climate events simultaneous between Greenland and France? A quantitative comparison using non-tuned chronologies. *J. Quat. Sci.* 25, 387–394.
- Celle-jeanton, H., Travi, Y., Blavoux, B., 2001. Isotopic typology of the precipitation in the Western Mediterranean region at three different time scales. *Geophys. Res. Lett.* 28, 1215–1218.
- Comas-Bru, L., McDermott, F., 2014. Impacts of the EA and SCA patterns on the European twentieth century NAO–winter climate relationship. *Q. J. R. Meteorol. Soc.* 140, 354–363.
- Craig, H., 1961. Isotopic variations in meteoric waters. *Science* 133, 1702–1703.
- Dansgaard, W., 1964. Stable isotopes in precipitation. *Tellus* 16, 436–468.
- Dominguez-Villar, D., Wang, X., Krklec, K., Cheng, H., Edwards, R.L., 2017. The control of the tropical North Atlantic on Holocene millennial climate oscillations. *Geology* 45, 303–306.
- Feurdean, A., Perşoiu, A., Pazdur, A., Onac, B.P., 2011. Evaluating the palaeoecological potential of pollen recovered from ice in caves: a case study from Scărișoara Ice Cave, Romania. *Rev. Palaeobot. Palynol.* 165, 1–10.
- Fletcher, W.J., Debret, M., Sanchez Goñi, M.F., 2013. Mid-Holocene emergence of a low-frequency millennial oscillation in western Mediterranean climate: implications for past dynamics of the North Atlantic atmospheric westerlies. *Holocene* 23, 153–166.
- Fletcher, W.J., Zielhofer, C., 2013. Fragility of Western Mediterranean landscapes during Holocene rapid climate changes. *Catena* 103, 16–29.
- González-Sampériz, P., Aranbarri, J., Pérez-Sanz, A., Gil-Romera, G., Moreno, A., Leunda, M., Sevilla-Callejo, M., Corella, J.P., Morellón, M., Oliva, B., Valero-Garcés, B., 2017. Environmental and climate change in the southern Central Pyrenees since the last Glacial maximum: a view from the lake records. *Catena* 149, 668–688.
- Gómez-Lende, M., Berenguer, F., Serrano, E., 2014. Morphology, ice types and thermal regime in a high mountain ice cave. First studies applying terrestrial laser scanner in the Peña Castil Ice Cave (Picos de Europa, Northern Spain). *Geogr. Fis. Din. Quat.* 37, 141–150.
- Gradziński, M., Hercman, H., Peresviet-Soltan, A., Zelinka, J., Jelonek, M., 2016. Radiocarbon dating of fossil bats from Dobšina Ice Cave (Slovakia) and potential palaeoclimatic implications. *Ann. Soc. Geol. Pol.* 86, 341–350. <https://doi.org/10.14241/asgp.2016.016>.
- Hercman, H., Gąsiorowski, M., Gradziński, M., Kicińska, D., 2010. The first dating of cave ice from Tatra Mountains, Poland and its implication to palaeoclimate reconstructions. *Geochronometria* 36, 31–38.
- Jódar, J., Custodio, E., Lambán, L.J., Martos-Rosillo, S., Herrera-Lameli, C., Sapriza-Azuri, G., 2016. Vertical variation in the amplitude of the seasonal isotopic content of rainfall as a tool to jointly estimate the groundwater recharge zone and transit times in the Ordesa and Monte Perdido National Park aquifer system, North–Eastern Spain. *Sci. Total Environ.* 573, 505–517.
- Kern, Z., Fórizs, I., Pavuza, R., Molnár, M., Nagy, B., 2011. Isotope hydrological studies of the perennial ice deposit of Saarlhale, Mammuthöhle, Dachstein Mts, Austria. *Cryosphere* 5, 291–298.
- Kern, Z., Molnár, M., Svingor, É., Perşoiu, A., Nagy, B., 2009. High resolution, well preserved tritium record in the ice of Borțig Ice Cave, Bihor Mountains, Romania. *Holocene* 19, 729–736. <https://doi.org/10.1177/0959683609105296>.
- Kern, Z., Perşoiu, A., 2013. Cave ice – the imminent loss of untapped mid-latitude cryospheric palaeoenvironmental archives. *Quat. Sci. Rev.* 67, 1–7.
- Lauriol, B., Clark, I., 1993. An approach to determine the origin and age of massive ice blockage in two arctic caves. *Permafrost. Periglac. Process.* 4, 77–85.
- López-Moreno, J.J., Vicente-Serrano, S.M., Morán-Tejeda, E., Lorenzo-Lacruz, J., Kenawy, A., Beniston, M., 2011. Effects of the North Atlantic Oscillation (NAO) on combined temperature and precipitation winter modes in the Mediterranean mountains: observed relationships and projections for the 21st century. *Glob. Planet. Change* 77, 62–76.
- Luetscher, M., Bolius, D., Schwikowski, M., Schotterer, U., Smart, P.L., 2007. Comparison of techniques for dating of subsurface ice from Monlesli ice cave, Switzerland. *J. Glaciol.* 53, 374–384.

- Luetscher, M., Jeannin, P.Y., 2004. A process-based classification of alpine ice caves. *Theor. Appl. Karstology* 17, 5–10.
- Luetscher, M., Jeannin, P.Y., Haeberli, W., 2005. Ice caves as an indicator of winter climate evolution – a case study from the Jura Mountains. *Holocene* 15, 982–993.
- Mauri, A., Davis, B.A.S., Collins, P.M., Kaplan, J.O., 2015. The climate of Europe during the Holocene: a gridded pollen-based reconstruction and its multi-proxy evaluation. *Quat. Sci. Rev.* 112, 109–127.
- May, B., Spötl, C., Wagenbach, D., Dublyansky, Y., Liebl, J., 2011. First investigations of an ice core from Eisriesenwelt cave (Austria). *Cryosphere* 5, 81–93.
- Mayewski, P.A., Rohling, E.E., Curt Stager, J., Karlen, W., Maasch, K.A., David Meeker, L., Meyerson, E.A., Gasse, F., van Kreveland, S., Holmgren, K., Lee-Thorp, J., Rosqvist, G., Rack, F., Staubwasser, M., Schneider, R.R., Steig, E.J., 2004. Holocene climate variability. *Quat. Res.* 62, 243–255.
- Morellón, M., Valero-Garcés, B., Anselmetti, F., Ariztegui, D., Schnellmann, M., Moreno, A., Mata, P., Rico, M., Corella, J.P., 2009. Late Quaternary deposition and facies model for karstic Lake Estanya (North-eastern Spain). *Sedimentology* 56, 1505–1534.
- Morellón, M., Pérez-Sanz, A., Corella, J.P., Büntgen, U., Catalán, J., González-Sampériz, P., González-Trueba, J.J., López-Sáez, J.A., Moreno, A., Pla-Rabes, S., Saz-Sánchez, M.Á., Scussolini, P., Serrano, E., Steinhilber, F., Stefanova, V., Vegas-Vilarrúbia, T., Valero-Garcés, B., 2012. A multi-proxy perspective on millennium-long climate variability in the Southern Pyrenees. *Clim. Past* 8, 683–700.
- Pelachs, A., Julia, R., Perez-Obiol, R., Soriano, J.M., Bal, M.-C., Cunill, R., Catalan, J., 2011. Potential influence of Bond events on mid-Holocene climate and vegetation in southern Pyrenees as assessed from Burg Lake LOI and pollen records. *Holocene* 21, 95–104.
- Pérez-Sanz, A., González-Sampériz, P., Moreno, A., Valero-Garcés, B., Gil-Romera, G., Rieradevall, M., Tarrats, P., Lasheras-Álvarez, L., Morellón, M., Belmonte, A., Sancho, C., Sevilla-Callejo, M., Navas, A., 2013. Holocene climate variability, vegetation dynamics and fire regime in the Central Pyrenees: the Basa de la Mora sequence (NE Spain). *Quat. Sci. Rev.* 73, 149–169.
- Perşoiu, A., Onac, B.P., 2012. Ice in caves. In: White, W.B., Culler, D.C. (Eds.), *Encyclopedia of Caves*. Academic Press, Elsevier Inc., pp. 399–404.
- Perşoiu, A., Onac, B.P., Wynn, J.G., Blaauw, M., Ionita, M., Hansson, M., 2017. Holocene winter climate variability in Central and Eastern Europe. *Sci. Rep.* 7, 1196. <https://doi.org/10.1038/s41598-017-01397-w>.
- Perşoiu, A., Onac, B.P., Wynn, J.G., Bojar, A.V., Holmgren, K., 2011. Stable isotope behavior during cave ice formation by water freezing in Scărișoara Ice Cave, Romania. *J. Geophys. Res.* 116, D02111. <https://doi.org/10.1029/2010JD014477>.
- Pla, S., Catalan, J., 2005. Chrysophyte cysts from lake sediments reveal the sub-millennial winter/spring climate variability in the northwestern Mediterranean region throughout the Holocene. *Clim. Dyn.* 24, 263–278.
- Reimer, P., Bard, E., Bayliss, A., Beck, J., Blackwell, P., Bronk Ramsey, C., Grootes, P., Guilderson, T., Hafflidason, H., Hajdas, I., Hatt, Z.C., Heaton, T., Hoffmann, D., Hogg, A., Hughen, K., Kaiser, K., Kromer, B., Manning, S., Niu, M., Reimer, R., Richards, D., Scott, E., Southon, J., Staff, R., Turney, C., van der Plicht, J., 2013. IntCal13 and Marine13 radiocarbon age calibration curves 0–50,000 years cal BP. *Radiocarbon* 55, 1869–1887.
- Rozanski, K., Araguás-Araguás, L., Gonfiantini, R., 1993. Isotopic patterns in modern global precipitation. *Geophys. Monogr. Ser.* 78, 1–36.
- Ruan, J., Kherbouche, F., Genty, D., Blamart, D., Cheng, H., Dewilde, F., Hachi, S., Edwards, R.L., Régnier, E., Michelot, J.-L., 2016. Evidence of a prolonged drought ca. 4200 yr BP correlated with prehistoric settlement abandonment from the Guedaman GLD1 Cave, Northern Algeria. *Clim. Past* 12, 1–14.
- Schürch, M., Kozel, R., Schotterer, U., Tripet, J.P., 2003. Observation of isotopes in the water cycle – the Swiss National Network (NISOT). *Environ. Geol.* 45, 1–11.
- Spötl, C., Reimer, P.J., Luetscher, M., 2014. Long-term mass balance of perennial firn and ice in an Alpine cave (Austria): constraints from radiocarbon-dated wood fragments. *Holocene* 24, 165–175.
- Stoffel, M., Luetscher, M., Bollschweiler, M., Schlatter, F., 2009. Evidence of NAO control on subsurface ice accumulation in a 1200 yr old cave-ice sequence, St. Livres ice cave, Switzerland. *Quat. Res.* 72, 16–26.
- Trigo, R.M., Osborn, T.J., Corte-Real, J.M., 2002. The North Atlantic Oscillation influence on Europe: climate impacts and associated physical mechanisms. *Clim. Res.* 20, 9–17.
- Wassenburg, J.A., Dietrich, S., Fietzke, J., Fohlmeister, J., Jochum, K.P., Scholz, D., Richter, D.K., Sabaoui, A., Spötl, C., Lohmann, G., Andreae, M.O., Immenhauser, A., 2016. Reorganization of the North Atlantic Oscillation during early Holocene deglaciation. *Nat. Geosci.* 9, 602–605.
- Yonge, C.J., MacDonald, W.D., 2014. Stable isotope composition of perennial ice in caves as an aid to characterizing ice cave types. In: Land, L., Kern, Z., Maggi, V., Turri, S. (Eds.), 6th International Workshop on Ice Caves. NCKRI Symposium 4. National Cave and Karst Research Institute, Carlsbad, NM, USA, pp. 41–49.
- Zielhofer, C., Fletcher, W.J., Mischke, S., De Batist, M., Campbell, J.F.E., Joannin, S., Tjallingii, R., El Hamouti, N., Junginger, A., Stele, A., Bussmann, J., Schneider, B., Lauer, T., Spitzer, K., Strupler, M., Brachert, T., Mikdad, A., 2017. Atlantic forcing of Western Mediterranean winter rain minima during the last 12,000 years. *Quat. Sci. Rev.* 157, 29–51.